Parasitology

cambridge.org/par

Trichostatin A induces *Trypanosoma cruzi* histone and tubulin acetylation: effects on cell division and microtubule cytoskeleton remodelling

Jean de Oliveira Santos[1,2,*], Aline Araujo Zuma[1,2,*], Francisca Nathalia de Luna Vitorino[3], Julia Pinheiro Chagas da Cunha[3], Wanderley de Souza[1,2] and Maria Cristina M. Motta[1,2]

[1]Laboratório de Ultraestrutura Celular Hertha Meyer, Instituto de Biofísica Carlos Chagas Filho, Universidade Federal do Rio de Janeiro-UFRJ, 21491-590, Rio de Janeiro, RJ, Brazil; [2]Instituto Nacional de Ciência e Tecnologia e Núcleo de Biologia Estrutural e Bioimagens – CENABIO, UFRJ, RJ, Brazil and [3]Laboratório Especial de Ciclo Celular, Center of Toxins, Immune Response and Cell Signaling – CeTICS, Instituto Butantan, São Paulo, 05503-900, SP, Brazil

Research Article

*Both authors contributed equally to this scientific article.

Cite this article: de Oliveira Santos J, Zuma AA, de Luna Vitorino FN, da Cunha JPC, de Souza W, Motta MCM (2019). Trichostatin A induces *Trypanosoma cruzi* histone and tubulin acetylation: effects on cell division and microtubule cytoskeleton remodelling. *Parasitology* **146**, 543–552. https://doi.org/10.1017/S0031182018001828

Received: 2 July 2018
Revised: 30 September 2018
Accepted: 1 October 2018
First published online: 13 November 2018

Key words:
Acetylation; histone; histone deacetylases inhibitor (HDACi); microtubule cytoskeleton; trichostatin A (TSA); *Trypanosoma cruzi*; tubulin

Author for correspondence:
Maria Cristina M. Motta,
E-mail: motta@biof.ufrj.br

Abstract

Trypanosoma cruzi, the causative agent of Chagas disease, is a public health concern in Latin America. Epigenetic events, such as histone acetylation, affect DNA topology, replication and gene expression. Histone deacetylases (HDACs) are involved in chromatin compaction and post-translational modifications of cytoplasmic proteins, such as tubulin. HDAC inhibitors, like trichostatin A (TSA), inhibit tumour cell proliferation and promotes ultrastructural modifications. In the present study, TSA effects on cell proliferation, viability, cell cycle and ultrastructure were evaluated, as well as on histone acetylation and tubulin expression of the *T. cruzi* epimastigote form. Protozoa proliferation and viability were reduced after treatment with TSA. Quantitative proteomic analyses revealed an increase in histone acetylation after 72 h of TSA treatment. Surprisingly, results obtained by different microscopy methodologies indicate that TSA does not affect chromatin compaction, but alters microtubule cytoskeleton dynamics and impair kDNA segregation, generating polynucleated cells with atypical morphology. Confocal fluorescence microscopy and flow cytometry assays indicated that treated cell microtubules were more intensely acetylated. Increases in tubulin acetylation may be directly related to the higher number of parasites in the G2/M phase after TSA treatment. Taken together, these results suggest that deacetylase inhibitors represent excellent tools for understanding trypanosomatid cell biology.

Introduction

Trypanosoma cruzi, the aetiological agent of Chagas disease, presents special features when compared with other eukaryotes, like a single mitochondrion that presents interlocked DNA circles (kDNA) contained in the kinetoplast and a typical cytoskeleton array (Soares, 1999; De Souza, 2002). The arrangement of trypanosomatid cytoskeleton is simpler than those of most other eukaryotic cells; however, it is precisely organized and constituted by stable microtubules. Such microtubules compose the mitotic spindle, the basal body, the flagellar axoneme and the subpellicular microtubules, which are connected to each other and also to the plasma membrane, thus forming a helical arrangement along the central axis of the trypanosomatid cell body (Souto-Padron *et al.*, 1993; Schneider *et al.*, 1997; Kohl and Gull, 1998; Alonso *et al.*, 2016; Vidal and De Souza, 2017).

As in other eukaryotes, trypanosomatid microtubules are formed by α/β-tubulin heterodimers, comprising 13 typical protofilaments connected to each other (Vidal and De Souza, 2017). In *Trypanosoma brucei*, the microtubule plus ends, more dynamic in tubulin polymerization/depolymerization, are found in the posterior end of the cell body. Microtubules are more stable in the protozoan anterior end that contains the flagellum, emerging from the basal body, which is physically linked to the kinetoplast (Robinson *et al.*, 1995).

The microtubules and tubulin undergo several post-translational modifications (PTMs), such as phosphorylation, glycosylation, ubiquitination, methylation and acetylation, which influence microtubule dynamics, organization, as well as cell differentiation and motility (Song and Brady, 2015; Wloga *et al.*, 2017). Tubulin was the first non-histone protein to be discovered as a PTMs target. Acetylation on Lys40 (K40) of α-tubulin is conserved from lower eukaryotes to mammals (L'hernault and Rosenbaum, 1985) and was associated for a long time with microtubule stability. This statement led to a controversial issue: does tubulin acetylation stabilize microtubules or is tubulin acetylated once it is stable? Currently, the second hypothesis is accepted as correct. It is also known that K40 acetylation occurs significantly on flagella, centrioles, cilia, basal body and the mitotic spindle (Piperno and Fuller, 1985; Cambray-Deakin and Burgoyne, 1987; Szyk *et al.*, 2014; Sadoul and Khochbin, 2016).

CAMBRIDGE UNIVERSITY PRESS

Tubulin acetylation is better known in higher eukaryotes. In *T. cruzi*, molecular analyses identified two homologous sequences for tubulin-acetyltransferases (Alsford and Horn, 2011). Regarding deacetylases, SIR2 RP1 in *Leishmania major* was the first sirtuin (SIRT) homologue reported in trypanosomatids. Similarly to human SIRT2 and histone deacetylase 6 (HDAC6), SIR2 RP1 associates with the microtubule cytoskeleton and is able to deacetylase α-tubulin (Yahiaoui *et al.*, 1996; Tavares *et al.*, 2008). In *T. brucei*, SIR2 RP1 is located in the nucleus and is related to chromatin condensation and histone deacetylation (García-Salcedo *et al.*, 2003). According to the TriTryp gene bank, the *T. cruzi* genome presents two coding sequences for lysine deacetylases homologous to HDAC6 and two for sirtuins (http://tritrypdb.org/tritrypdb/). This parasite also presents the BDF3 protein, which plays a role in tubulin acetylation (Alonso and Serra, 2012; Alonso *et al.*, 2014).

Like tubulins, histones are also subject to several PTMs. In trypanosomatids, histones differ from their human counterparts regarding sequence, size and PTMs. In these parasites, histones are highly acetylated at the H2A C-terminus and contain multiple acetylation and methylation sites at the H4 and H3 N-terminus. Histone variants, such as H2Az and H2Bv, are also subject to PTMs (Thatcher and Gorovsky, 1994; Da Cunha *et al.*, 2006; Janzen *et al.*, 2006; De Jesus *et al.*, 2016).

Histone acetylation and deacetylation are epigenetic marks that require two classes of enzymes: histone acetyltransferases (HATs) and HDACs. When HATs add an acetyl group to a histone lysine residue, the lysine positive charge is neutralized, possibly reducing the association between the histone octamer and the DNA. This results in a more relaxed chromatin state associated with an increase in transcription activation. HDACs act by removing the acetyl group of histones, resulting in an increase in histone and DNA interaction, associated with chromatin compaction and transcription suppression (Alsford and Horn, 2004; Khorasanizadeh, 2004; Monneret, 2005; Legartová *et al.*, 2013; Angiolilli *et al.*, 2017).

Histones are not the exclusive target of HATs and HDACs, which can act on transcriptional factors, nuclear receptors, chaperones, cytoskeleton components and DNA binding proteins. In trypanosomatids, HDACs are related to cell cycle, transcriptional repression, euchromatin organization and the expression of the genes that encode variant surface glycoproteins in *T. brucei* (Alsford and Horn, 2004; Marks *et al.*, 2004; Monneret, 2005; Martinez-Iglesias *et al.*, 2008).

HDAC inhibitors (HDACi) have been widely used in chemotherapy against cancer and as a tool to understand the roles of these enzymes. Trichostatin A (TSA) is a derivative of hydroxamic acid isolated from *Streptomyces hygroscopicus* and first characterized as an anti-fungal agent (Tsuji *et al.*, 1976; Marks *et al.*, 2004; Campo, 2017). This compound is able to bind irreversibly to the catalytic site of HDAC I and II, preventing their connection to histones and resulting in their hyperacetylation (Toth, 2004). TSA effects against cell proliferation, cell cycle progression and DNA condensation in tumour cell lines are well known, even when used in nanomolar concentrations (Martínez-Iglesias *et al.*, 2008; Legartová *et al.*, 2013).

Although TSA has been widely applied in studies with cancer cells, its effects on protozoan parasites, such as trypanosomatids, have been less exploited. In *T. cruzi*, TSA modulates the expression of genes required for division and differentiation, besides inhibiting metacyclogenesis, which is essential for parasite infectivity (Campo, 2017). In the present study, it is demonstrated that TSA affects *T. cruzi* proliferation and viability, also promoting cell cycle arrest in the G2/M phase. Here we show for the first time, that this compound increased acetylation not only in parasite histones but also in tubulin, thus promoting microtubule cytoskeleton remodelling.

Material and methods

Trypanosoma cruzi culture

Epimastigote forms of *T. cruzi* Y were grown at 28 °C in liver infusion tryptose medium (Camargo, 1964) supplemented with 10% fetal calf serum for 3 days, corresponding to the growth exponential time.

Anti-trypanosomal activity assays

TSA (Sigma-Aldrich, Germany) was diluted in dimethyl sulphoxide (DMSO), obtaining a 5 mM stock solution. To verify inhibitor effects on *T. cruzi*, the compounds were applied at 1, 5, 10, 50 and 100 μM for up to 72 h. The concentration of DMSO used was equivalent to the highest concentration of TSA. Parasites were collected every 24 h for counting in a Neubauer chamber. To compare the controls and the treated groups, paired *t*-tests were applied to the results at a 95% confidence interval (GraphPad Prism version 5.00 for Windows; GraphPad Software Inc., San Diego, CA, USA). To evaluate protozoa viability in the presence of the above-mentioned inhibitors, parasites were incubated with MTS [3-(4,5-dimethylthiazol-2-yl)-5-(3-carboxymethoxyphenyl)-2-(4-sulfophenyl)-2H-tetrazolium] and PMS (phenazine methosulphate) (Promega) for 4 h (Henriques *et al.*, 2011). Untreated parasites were fixed in 0.4% formaldehyde for 10 min and used as the negative control. The percentage of viable parasites was obtained through a spectrofluorometer (Molecular Devices Microplate Reader, SpectraMax M2/M2e, Molecular Devices, USA) at 490 nm. This analysis was performed by three independent experiments each one performed in duplicate.

Fluorescence light microscopy

To assess the occurrence of multinucleated parasites, cells were washed in PBS and fixed in 4% formaldehyde in PBS for 5 min and then deposited on slides previously coated with poly-L-lysine for 10 min and incubated with 4′,6-diamidino-2-phenylindole (DAPI, from Molecular Probes, USA) diluted at 1:500 for 5 min. The slides were then washed, mounted in ProLong Gold Antifade Mountant (Thermo Fisher Scientific, USA) and observed under Leica TCS-SPE (63× objective and 405 nm laser) and Elyra PS.1 (100× objective and 405 nm laser) microscopes. To determine the percentage of polynucleated parasites, 200 cells were counted. This analysis was performed by two independent experiments.

Immunofluorescence microscopy

To evaluate TSA effects on tubulin and acetylated tubulin expression, protozoa were washed in PBS and fixed and deposited on slides as previously described. Subsequently, parasites were incubated for 30 min in a blocking solution containing 3% bovine serum albumin, 0.5% teleostean gelatin (Sigma-Aldrich) and 1% saponin diluted in PBS (pH 8.0). The slides containing the cells were then incubated with antibodies against tubulin (1:100) (Sigma-Aldrich T5168) and acetylated tubulin (1:150) (Sigma-Aldrich T7451) overnight. The parasites were washed and incubated for 45 min with Alexa Fluor® 488 and Alexa Fluor® 546 (1:400) (Thermo Fisher Scientific). Samples were also incubated with DAPI for 5 min. The slides were then mounted and observed under Leica TCS-SPE (63× objective, 405 and 532 nm lasers) and Elyra PS.1 (100× objective, 405 and 543 nm lasers) microscopes. This analysis was performed by two independent experiments.

Cell cycle analysis by flow cytometry

To analyse the progression of the *T. cruzi* cell cycle during treatment with TSA, parasites were fixed in 1 mL of 0.25%

https://doi.org/10.1017/S0031182018001828 Published online by Cambridge University Press

formaldehyde in PBS for 5 min, and then washed and resuspended in 70% cold ethanol for 30 min. Subsequently, cells were washed and incubated with 5 μM SYTOX® Green (Invitrogen, USA) for 30 min at room temperature. *Trypanosoma cruzi* was treated with 10 μM camptothecin (CPT) as a cell cycle blockade, control (Zuma, *et al.*, 2014). The analysis was performed on a BD Accuri C6 flow cytometer (Becton Dickinson Bioscience BDB, San Jose, CA, USA), and data were analysed by the BD Accuri C6 software. This analysis was performed by two independent experiments.

Tubulin expression analysis by flow cytometry

For the analyses of tubulin and acetylated tubulin expressions, control and TSA-treated parasites were fixed, permeabilized and incubated with specific antibodies as described previously in item 2.5. Protozoa were then resuspended in PBS and the analysis was performed as described in the above item. This analysis was performed by two independent experiments.

Transmission electron microscopy

To assess TSA effects on *T. cruzi* ultrastructure, protozoa were fixed in 2.5% glutaraldehyde diluted in 0.1 M cacodylate buffer (pH 7.2) for 1 h and then washed in the same buffer. Parasites were post-fixed in 1% osmium tetroxide and 0.8% potassium ferricyanide, diluted in the same buffer, for 1 h. After washing in cacodylate buffer, cells were dehydrated in a graded series of acetone and embedded in Epon (Electron Microscopy Sciences, Hatfield, PA, USA). Ultra-thin sections were stained with uranyl acetate for 40 min and lead citrate for 5 min. The samples were observed under a Zeiss 900 transmission electron microscope (Zeiss, Oberkochen, Germany). This analysis was performed by two independent experiments.

Ultrastructural cytochemical analysis using phosphotungstic acid

Parasites were fixed as described above, dehydrated in ethanol and then post-fixed as previously mentioned. Subsequently, cells were incubated for 2 h in a solution containing 2% phosphotungstic acid (PTA) diluted in absolute ethanol and embedded in Epon. Ultra-thin sections were stained and observed as described above. This analysis was performed by two independent experiments.

Negative staining technique

To assess TSA effects on *T. cruzi* microtubule cytoskeleton, parasites were centrifuged and resuspended in culture media. Following this, 8 μL of this suspension were added on formvar film-coated grids, previously submitted to glow discharge (PELCO easiGlow™, USA) for 30 s. Grids containing the adhered cells were incubated with 0.1 M PHEM buffer (5 mM HEPES, 60 mM PIPES, 10 mM EGTA, 2 mM MgCl2) and 1% NP-40 (Sigma-Aldrich) for 5 min. After that, parasites were fixed as described above in PHEM buffer for 10 min. Then, samples were washed three times with deionized water for 5 min and contrasted with 8 μL of 1% aurothioglucose diluted in deionized water. The grids were then placed onto a sheet of filter paper to remove excess water and immediately observed. This analysis was performed by two independent experiments.

Scanning electron microscopy

To study *T. cruzi* morphology in the presence of TSA, parasites were fixed as presented in item 2.9 and adhered to poly-L-lysine-coated microscope coverslips. The samples were post-fixed, dehydrated (as previously described), critical point dried in CO_2 and ion sputtered. The samples were observed under a Quanta X50 scanning electron microscope (SEM; FEI Company, The Netherlands). This analysis was performed by two independent experiments.

SEM after detergent membrane extraction

To analyse the organization of the *T. cruzi* microtubule cytoskeleton by SEM, parasites were washed in PHEM buffer, adhered to microscope coverslips and incubated with 1% NP-40 for 15–20 min at room temperature. Then, the samples were washed in PHEM and fixed for 20 min. Parasites were subjected to the same steps described above prior to viewing under the microscope. This analysis was performed by two independent experiments.

Quantitation of acetylated histones by LC-MS/MS

For proteomic analyses, protozoa were grown to a final concentration of 1×10^7 cells mL^{-1} in a total volume of 5 mL. After 24 h, parasites were treated with 100 μM of TSA or the equivalent volume of DMSO (control). Experiments were performed in triplicate. Cells were harvested after 72 h of treatment, washed in PBS solution and the pellets were then separated and kept at −80 °C.

Histones were extracted from the parasite pellets as described previously (De Jesus *et al.*, 2016). Briefly, chromatin was extracted (Toro and Galanti, 1990) and histones were acid-extracted by HCl 0.3 M. Protein samples were quantified by the bicinchoninic acid protein assay kit (Thermo Fisher, USA) and 10 μg of each sample were trypsin-digested as described previously (Villén and Gygi, 2008). Peptides were resuspended in 0.1% formic acid and fractionated on an in-house reversed phase capillary emitter column (10 cm × 75 μm, filled with 5 μm C18 Aqua resins-Phenomenex) coupled to a nanoHPLC (1D plus – Proxeon). Fractionation was carried out on a 60 min gradient of 5–35% of acetonitrile in 0.1% formic acid followed by a 5 min gradient of 40–95% at a flow rate of 200 nL min^{-1}. The eluted peptides were analysed by a LTQ-Orbitrap Velos (Thermo Scientific) (source voltage – 1.9 kV, capillary temperature – 200 °C) in data-dependent mode, where each full mass spectrometry (MS) scan (200–2000 *m/z* range) was followed by 10 MS/MS (from the most intense ions). The resolution was set as 30 000 and normalized collision energy at 35. Data were processed and analysed by the MaxQuant software (1.5.8.0). Searches were performed against a database containing all *T. cruzi* histones (57 sequences) downloaded at http://tritrypdb.org/tritrypdb/. Variable modifications were set as acetylation (N-terminus and K), methylation (K and R), demethylation (K and R) and trimethylation (K). MS1 (first stage of MS) tolerance was set at 10 ppm and MS2 (second stage of MS) of 0.5 Da. False discovery rate was set as 1%. Proteins classified as contaminants were removed from further analysis. A *t*-test was used for statistical analysis of acetylated peptides. For this end, intensity values (from protein groups output files) of acetylated peptides were normalized against the corresponding total histone content detected by LFQ values as performed previously (De Jesus *et al.*, 2016). This analysis was performed by three independent experiments.

Statistical analyses

The statistical analyses were performed using two-way analysis of variance (ANOVA) and Bonferroni post-tests in the GraphPad Prism 7.0 software, with significance set at $P < 0.05$.

https://doi.org/10.1017/S0031182018001828 Published online by Cambridge University Press

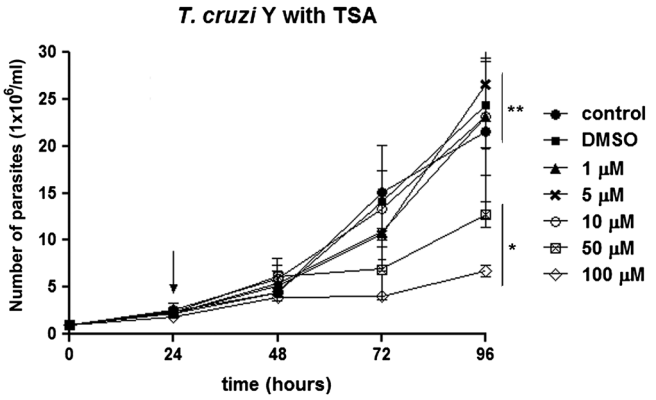

Fig. 1. *Trypanosoma cruzi* epimastigote proliferation in the presence of TSA. The drug was added to the medium after 24 h of growth (arrow). The higher concentrations (50 and 100 μM) inhibited parasite proliferation after 72 h of treatment. These data are the average of three independent experiments performed in duplicate. Two-way ANOVA and Bonferroni post-tests were performed considering $^{*}P < 0.05$ and $^{**}P > 0.05$.

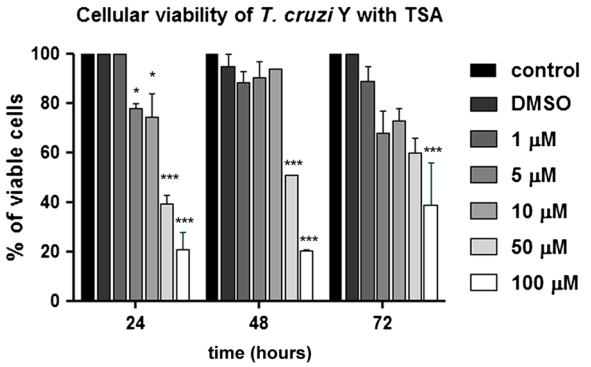

Fig. 2. Analysis of *T. cruzi* epimastigote viability in the presence of TSA using the MTS/PMS method. The 50 and 100 μM concentrations promoted the highest reduction in cell viability. After 24 h in the presence of the compound, the percentage of viable parasites decreased to 40 and 21%, respectively. This graph represents the average of three independent experiments, in triplicate. Two-way ANOVA and Bonferroni post-tests were performed considering $^{*}P < 0.05$ and $^{***}P < 0.001$.

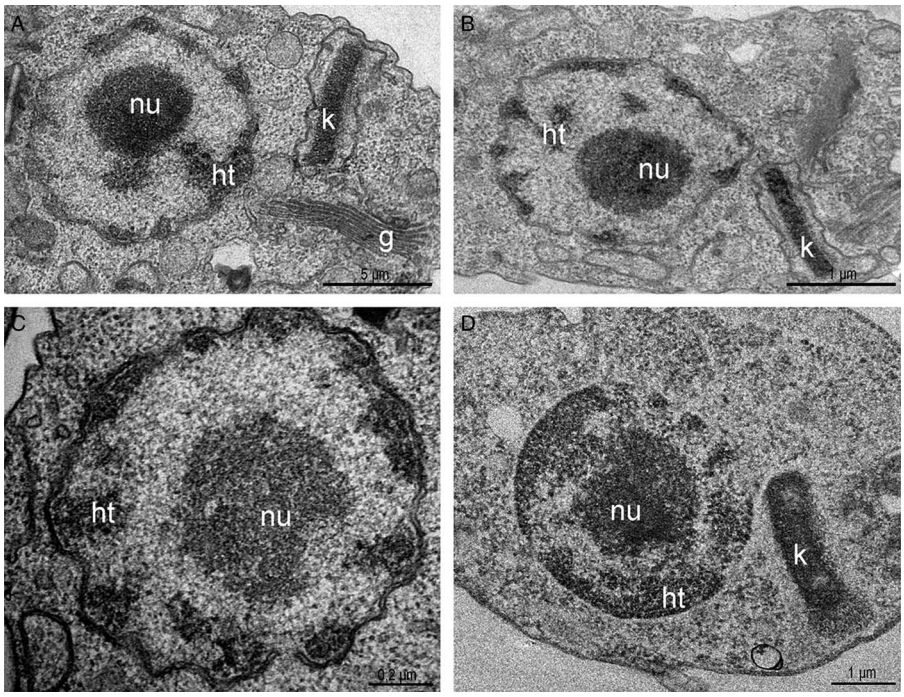

Fig. 3. Transmission electron micrograph of *T. cruzi* epimastigotes treated or not with trichostatin A. (A) Control parasites. Note the nucleus containing the nucleolus (nu) in the central region and the heterochromatin (ht) compacted in the periphery. The kinetoplast (k) presented the typical epimastigote bar shape and contained the kDNA with the characteristic arrangement. (B–C) Epimastigotes treated with 5 and 50 μM for 72 h of TSA, respectively. (D) The PTA technique did not evidence alterations in nuclear or mitochondrial DNA compaction even after treatment with 100 μM for 72 h of the inhibitor. g, Golgi complex.

Results

The effect of TSA on *T. cruzi* epimastigote proliferation was the first aspect evaluated herein. Parasite growth was inhibited by 46 and 58% after treatment with 50 and 100 μM TSA for 72 h, respectively. After applying lower concentrations of this inhibitor, such as 1, 5 and 10 μM, no significant decrease in cell proliferation was observed ($P > 0.05$), even after a long period of treatment. The IC_{50} value obtained after 72 h of treatment was 60 μM (Fig. 1).

Concerning cell viability, TSA caused a decrease in the number of viable parasites even when low concentrations were applied ($P < 0.05$). Thus, treatment with 5 and 10 μM for 24 h reduced parasite viability in 22 and 26%. Higher doses, such as 50 and 100 μM, led to 60 and 79% reduction in cell viability after the same treatment period ($P < 0.001$). Protozoa incubation at the highest concentration (100 μM) for 72 h indicated that approximately 50% of treated cells were viable, suggesting a recovery of *T. cruzi* epimastigote viability (Fig. 2).

Considering TSA effects on parasite proliferation and viability, the next step was to investigate if parasite ultrastructure was

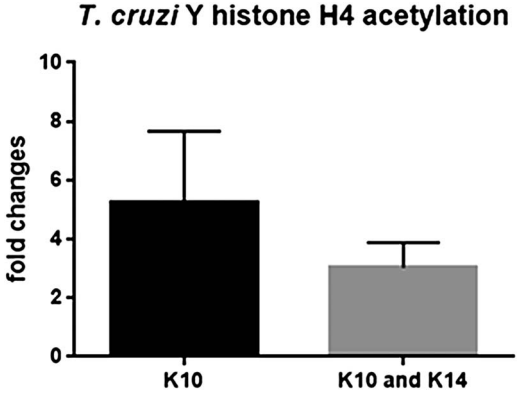

Fig. 4. *Trypanosoma cruzi* histone acetylation in the presence of TSA. After 72 h, acetylation at H4K10 and H4K10K14 was 5.4- and 3.02-fold higher, respectively, when compared with non-treated parasites. These data are the average of three independent experiments. Two-way ANOVA and Bonferroni post-tests were performed considering $^{*}P < 0.05$ and $^{**}P < 0.01$.

https://doi.org/10.1017/S0031182018001828 Published online by Cambridge University Press

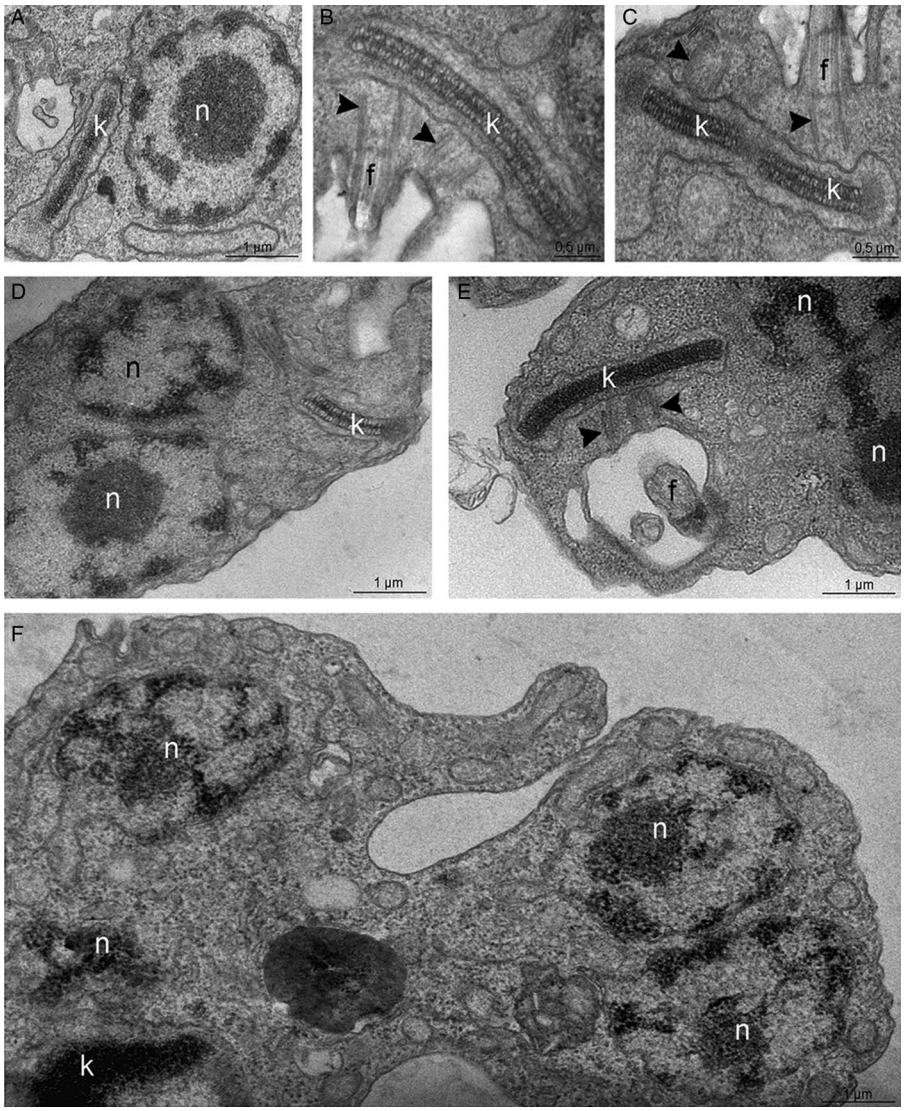

Fig. 5. Transmission electron microscopy for the ultrastructural analysis of the *T. cruzi* epimastigote form. (A–C) In control parasites, the nucleus (n) contains the nucleolus (nu) in the central region while heterochromatin (ht) is mainly observed in the nuclear periphery. The kinetoplast (k) presents the typical bar shape and contains the kDNA with the characteristic arrangement of epimastigotes. (B–C) In control cells, the kDNA duplicates and segregates attached to the basal bodies (arrowheads), which move apart during this process. (D–F) In parasites treated with 100 μM TSA, the duplicated kDNA is not segregated and doubled basal bodies are observed close to each other (arrowheads). As consequence, some cells present a single kinetoplast and multiple nuclei. g, Golgi complex.

affected. Thus, cells were treated with different concentrations of the inhibitor for 72 h and analysed by transmission electron microscopy (TEM). Control parasites presented a spherical nucleus, with a central electron-dense region corresponding to the nucleolus, and condensed heterochromatin close to the nuclear envelope. The kinetoplast was observed in its characteristic bar shape, containing a condensed kDNA (Fig. 3A). When parasites were treated with TSA, even at high concentrations for long periods, no nuclear ultrastructural alterations were observed, opposite of what was expected, since it is well described that this inhibitor can affect DNA compaction and organization (Fig. 3B and C). kDNA topology was not affected either (Fig. 3B). Considering that the use of low TSA concentrations for short periods did not affect DNA packing, we have privileged analyses after long treatment with the highest drug concentration (100 μM for 72 h). In such conditions, signs of cell death were not observed and approximately 40% of protozoa were viable.

In a next step, TSA-treated cells were submitted to the PTA ultrastructural cytochemistry technique that reveals basic proteins, such as histones, to possibly observe heterochromatin unpacking. However, no evidence of nuclear DNA or kDNA unpacking was observed using this cytochemical approach (Fig. 3D). In order to verify this hypothesis, histone PTMs were evaluated in more details. Briefly, histones were extracted from control cells and from parasites treated for 72 h with 100 μM TSA and analysed by LC-MS/MS. All histones were detected by MS with similar quantitative results in both conditions, indicating that TSA treatment did not alter their overall levels (no significant statistical difference). LFQ values in control *vs* TSA-treated samples for H2AZ + / − SEM: 2.6×10^8 + / − 1.9×10^7 and 3.2×10^8 + / − 1.6×10^7, respectively; LFQ values in control and TSA-treated samples for H4 + / − SEM: 2.6×10^9 + / − 1.6×10^8 and 3.0×10^9 + / − 2.3×10^8, respectively.

Acetylated histone peptides were detected and quantified for histone H4 (two sites), H2AZ (3 sites) and H1 (1 site). Interestingly, acetylation was enhanced in different histone types and sites after 72 h treatment with 100 μM TSA (Fig. 4). Acetylation of H4K10 (H4K10ac/total H4 + / − SEM for control: 6.9×10^{-5} + / − 2.3×10^{-5}; and for 100 μM TSA: 2.6×10^{-4} + / − 2.7×10^{-5}) and H4K10K14 (H4K10K14ac/total H4 + / − SEM for control: 1.5×10^{-4} + / − 2.4×10^{-5}; and for 100 μM TSA: 4.2×10^{-4} + / − 6.9×10^{-5}) was increased, on average, 5.24- and 3.02-fold, respectively, upon TSA treatment. Increases in H2AZ acetylation were even more evident (quantitative intensity values + / − SEM: at residues 55 or 59: 2.5×10^5 + / − 1.3×10^5; at 32 or 36: 1.0×10^6 + / − 5.5×10^5 and at 168 or 169: 3.1×10^6 + / −2.7×10^5) since no acetylated peptides were observed in this histone at control samples. Histone H1 (TcCLB.509837.40) acetylated at residue 64 was detected only upon TSA treatment (quantitative intensity value of 1.1×10^6 + / − 1.3×10^4). Of note, fold changes for H2AZ and H1 acetylated peptides were not calculated since the corresponding acetylated peptide

https://doi.org/10.1017/S0031182018001828 Published online by Cambridge University Press

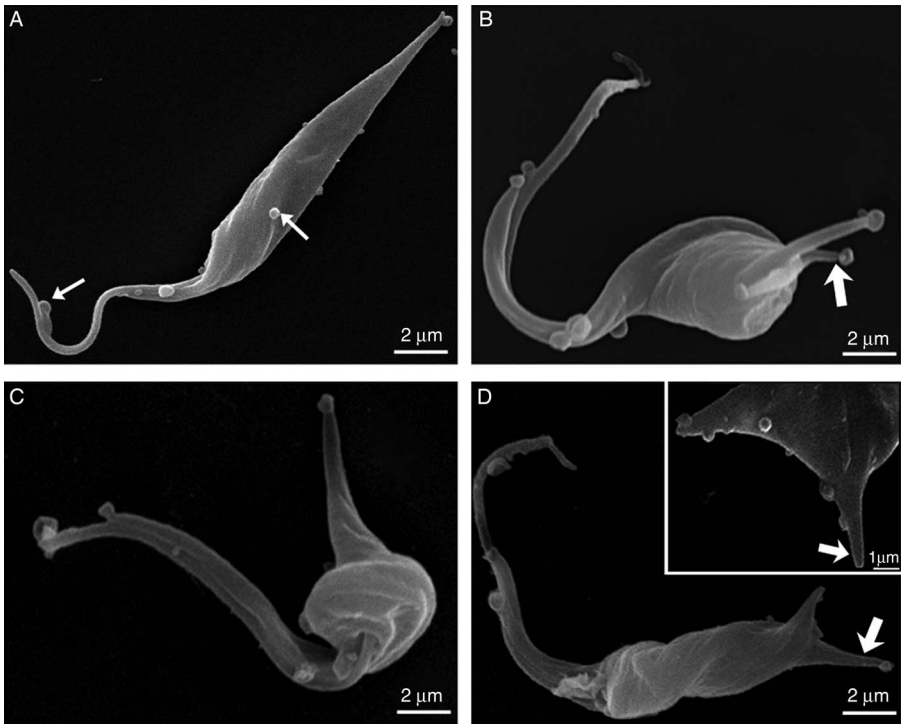

Fig. 6. Scanning electron micrographs of *T. cruzi* epimastigotes. (A) Non-treated cell. Note the elongated cell body with thinner posterior end and with the occurrence of vesicles at the cell surface (thin arrows). (B–D) After TSA treatment, epimastigotes developed distinctive phenotypes. (B) Cell presenting double cytoplasmic projections on the posterior end of the cell (arrow). (B–C) Rounding of the cell body at the central region and shortening of the parasite body. (D) Protozoan with cell body torsion. The inset shows a higher magnification of the cytoplasmic projections on the posterior end of the body (arrow).

was not detected at the control samples. Thus, even though no major ultrastructural alterations in nuclear DNA compaction were observed upon TSA treatment, histone acetylation was deeply affected.

The TEM analysis, interestingly, indicated that, contrary to control cells (Fig. 5A–C), parasites treated with 50 or 100 μM TSA for 72 h presented an atypical phenotype: basal bodies did not move apart during kDNA replication, resulting in abnormal protozoa presenting multiple nuclei and a single kinetoplast (Fig. 5D–F). Parasite morphology was also investigated by SEM in control- and TSA-treated cells. Non-treated epimastigotes presented a characteristic elongated cell body, thinner at the posterior end (Fig. 6A). TSA treatment led to the appearance of cytoplasmic projections at the posterior region of the parasite body, while the central area became rounded with protozoa presenting cell body shortening and torsion (Fig. 6B–D). The morphological changes described above corresponded to 32% of a total of 220 parasites. These results indicate that TSA could also affect tubulin acetylation that consequently promoted microtubule cytoskeleton remodelling. In order to explore this hypothesis, treated protozoa were analysed by combining different technical approaches.

First, the microtubule cytoskeleton of *T. cruzi* epimastigotes was investigated by the negative staining method. TEM images demonstrated that control cells presented the typical parallel array of subpellicular microtubules, extending from the anterior to the posterior end of the parasite (Fig. 7A). In TSA-treated protozoa, cells presented an atypical microtubule arrangement, where the distance between microtubules seemed to have increased, resulting in cell body enlargement (Fig. 7B and C), as previously observed by SEM (Fig. 6). Furthermore, the posterior end of the parasites was often disrupted (Fig. 7B) and some cells presented two nuclei and a single kinetoplast (Fig. 7C).

Analysis by confocal laser scanning microscopy demonstrated that parasites treated with 100 μM TSA for 72 h presented higher fluorescence intensity of the cell body and flagellum when labelled with anti-acetylated tubulin antibody compared with non-treated protozoa. It was interesting to observe that the posterior end of cells was faintly labelled, and the occurrence of multinucleated parasites was also observed (Fig. 8A–F). Protozoa treated with

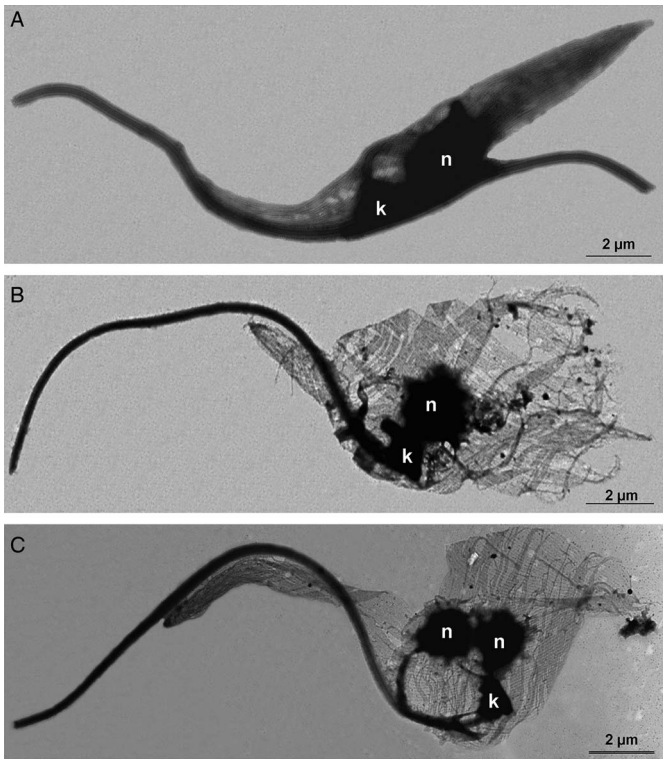

Fig. 7. Negative staining of *T. cruzi* epimastigotes after membrane removal by a detergent to evaluate the microtubule subpellicular corset organization. (A) Control parasite. Note the uniform organization of microtubules, regularly interspaced and maintaining their cell shape even after membrane extraction. (B–C) Cells treated with TSA 100 μM for 72 h. The parasite microtubule corset lacks its typical arrangement and becomes looser, especially at the posterior region of the cell. (C) Some parasites became multinucleated with a single kinetoplast after TSA treatment.

TSA containing two nuclei and one kinetoplast (2N1K) represented almost 8% of the culture, whereas this phenotype was observed in only 2% of non-treated parasites.

As a next step, the effect of TSA on tubulin acetylation was analysed by flow cytometry after labelling cells with

https://doi.org/10.1017/S0031182018001828 Published online by Cambridge University Press

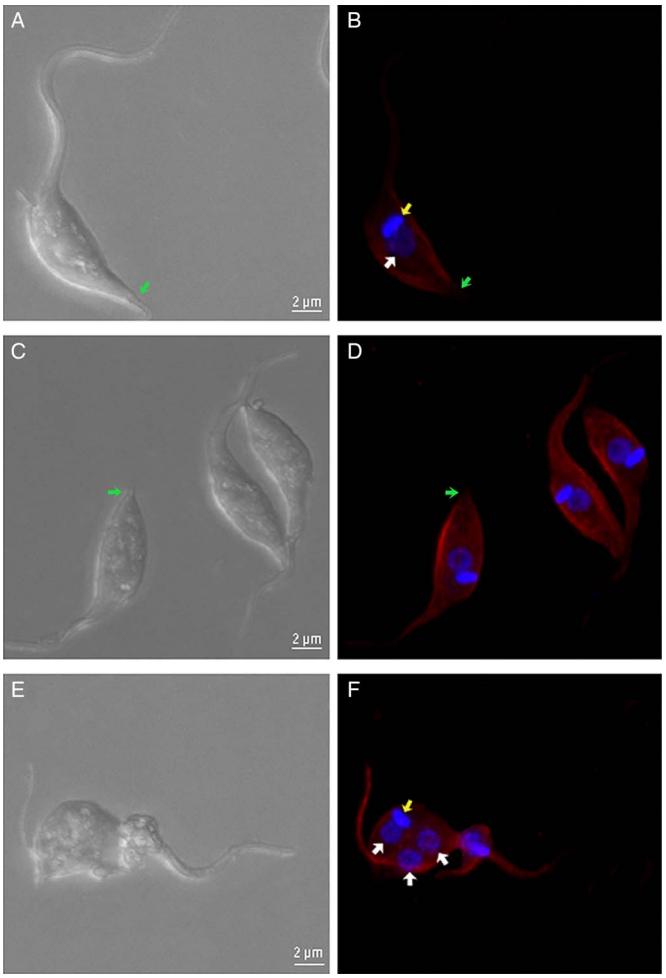

Fig. 8. Confocal fluorescence microscopy of control and TSA-treated parasites. (A), (C) and (E) DIC. (B), (D) and (F) parasites labelled with anti-acetylated tubulin antibodies and DAPI. (A and B) Non-treated cells. (C–F) Cells treated with 100 μM TSA. In treated parasites, an increase in the fluorescence intensity is evident when compared with control cells. Note that the extreme posterior region of the cells (arrows), which contains the more dynamic plus end microtubule region, remains unlabelled. (F) A multinucleated phenotype was also observed. Red – acetylated tubulin; blue – DAPI; white arrow – nucleus; yellow arrow – kinetoplast; green arrow – extreme posterior end.

anti-α-tubulin or anti-acetylated tubulin. When compared with non-treated cells, results indicated that parasite fluorescence intensity for total α-tubulin was enhanced after 24 h of treatment with 50 μM TSA by 68%, whereas the use of 100 μM of the inhibitor promoted an increase of 114%. Considering this same treatment period, values obtained for fluorescence intensity were augmented in 63 and 82% in cells labelled for acetylated tubulin after using 50 or 100 μM TSA, respectively (Fig. 9A). As the treatment of epimastigotes with TSA proceeded up to 72 h, these values increased as follows: approximately 45 and 201% after using 50 or 100 μM TSA, respectively, in cells labelled for total α-tubulin; 99 and 215% after applying 50 or 100 μM TSA, respectively, in protozoa labelled for acetylated tubulin (Fig. 9B). Taken together, these data reveal that TSA increases the amounts of α-tubulin and acetylated tubulin in a concentration and time-dependent manner.

Cell cycle progression was also investigated by flow cytometry considering the increased number of cells containing two nuclei and one kinetoplast (2N1K) after TSA treatment. In control cells, most parasites were in G1, as expected. Treatment with 50 μM TSA for up to 72 h did not affect significantly protozoa cell cycle. When 100 μM of the inhibitor was used for 24 h, the number of parasites in G2/M increased by 7% in relation to the control group. After 72 h in the presence of the same drug concentration, this percentage reached 15% (Fig. 10). As a positive control of cell cycle arrest, parasites were treated with 10 μM CPT since this compound is able to block the *T. cruzi* cell cycle at G2/M (ZUMA *et al.*, 2014). In this case, the percentage of cells in G2/M was 80% after treatment for 72 h.

Discussion

Chagas disease is a serious and neglected health problem in Latin America and currently represents an emerging illness in non-endemic countries. Since its discovery, a wide range of compounds has been tested against *T. cruzi*, the aetiological agent of this pathology. Among tested drugs, some target enzymes involved with PTMs. Histone acetylation has emerged as a main epigenetic mark that modifies gene expression, thus affecting cell division and influencing environment adaptation (Clayton and Shapira, 2007; Fan *et al.*, 2015). TSA is a HDACi that impairs the proliferation of tumour cell lines and human pathogens, such as *Plasmodium falciparum*, *T. brucei* and *Toxoplasma gondii*, being more effective against the two first species (Suzuki *et al.*, 2000; Jones-Brando *et al.*, 2003; Sheader *et al.*, 2004; Wu *et al.*, 2007; Zou *et al.*, 2008; Wilson *et al.*, 2013). In the present study, we demonstrated that treatment of *T. cruzi* epimastigotes with TSA was relatively ineffective in blocking cell proliferation, since the IC_{50} value was 60 μM after 72 h of treatment. This is in accordance with a previous report demonstrating that *T. cruzi* epimastigote growth belonging to the CL Brener strain were not affected after incubation with TSA (0.4 or 40 μM) for 3 days (Campo, 2017). Considering cell viability, 24 h TSA treatment led to an 80% reduction in the number of viable protozoa. However, after 72 h, the percentage of dead cells dropped to 44%, suggesting an ability of the parasite to revert mitochondrial damages over time, thus culminating in an increased number of viable protozoa. TSA is not a trypanocidal drug since it inhibits parasite proliferation instead of causing *T. cruzi* death. Considering MTS/PMS is based on mitochondrial activity, treated parasites present reduced mitochondrial activity but they are still able to proliferate. It is important to remember that trypanosomatids are capable of performing aerobic fermentation when the respiratory chain is inefficient (Cazzulo, 1992; Bringaud *et al.*, 2006). In tumour cells, TSA treatment decreased cellular viability in 60% when tested in synergy with 1 μM tubastatin A (TST), which specifically targets HDAC6 (Sun *et al.*, 2014; Chao *et al.*, 2015).

According to the literature, TSA is able to promote unpacking, or even fragmentation, of nuclear heterochromatin (Toth, 2004; Zou *et al.*, 2008). Contrary to what was expected, *T. cruzi* nuclear organization was not affected after treatment with TSA and DNA condensation level was preserved, as demonstrated by TEM. To the best of our knowledge, this was the first time that TSA effects on *T. cruzi* histone acetylation were deeply analysed and quantified. Previously, Campo demonstrated that this inhibitor also enhanced the acetylation of H4 and H2B histones in epimastigotes and trypomastigotes belonging to the CL Brener strain. However, this analysis was performed by Western-blot assays using commercial antibodies (Campo, 2017). In other human parasites, TSA was also shown to modulate gene expression in *Entamoeba histolytica* and *P. falciparum* (Ehrenkaufer *et al.*, 2007; Andrews *et al.*, 2012).

Some reports associating TSA with cytoskeleton remodelling are available. One demonstrated that F-actin rearrangement is necessary for TSA-induced apoptosis in HeLa human cervical cancer cells. This is related to the fact that cytoskeleton dynamism is required for tumour cell death and is also associated with drug resistance (Yang *et al.*, 2014). The effect of TSA on tubulin acetylation has been attributed to its inhibitory action on HDAC6

https://doi.org/10.1017/S0031182018001828 Published online by Cambridge University Press

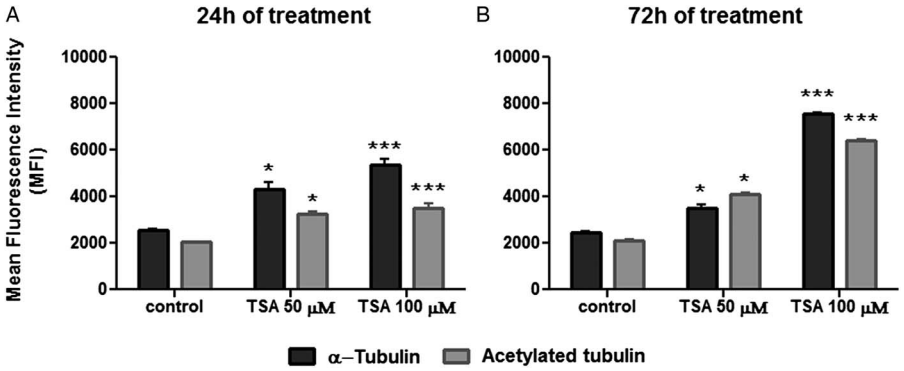

Fig. 9. Quantification of α-tubulin and acetylated tubulin labelling in control and TSA-treated cells. (A) Twenty-four hours TSA-treated cells. (B) Seventy-two hours TSA-treated cells. Two-way ANOVA and Bonferroni post-tests were performed considering $^{**}P < 0.01$ and $^{***}P < 0.001$.

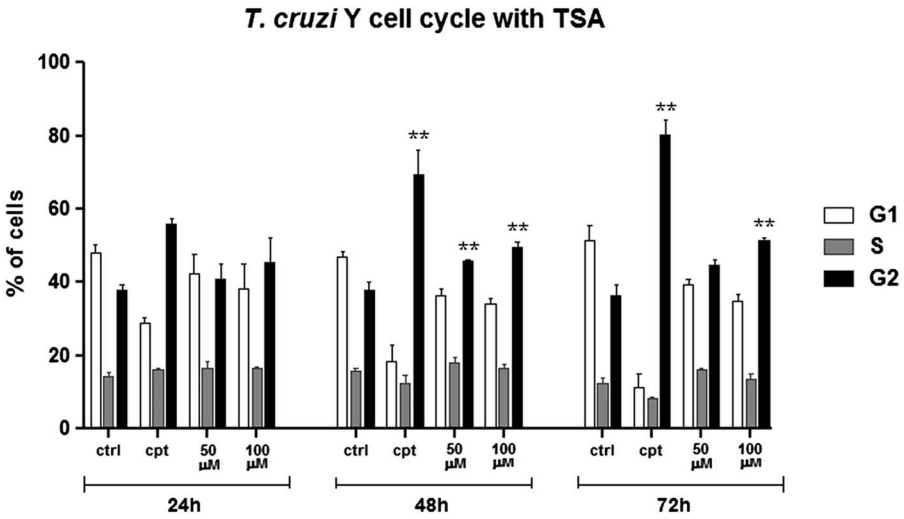

Fig. 10. Cell cycle progression after TSA treatment. Control cells presented a typical pattern of DNA amount throughout the cell cycle: most of the parasites are in G1, generating a higher peak, followed by a steep slope representing the cells in S and, lastly, a smaller than G1 peak representing the cells in G2. Camptothecin (Cpt), a positive control of cell cycle arrest in G2. Two-way ANOVA and Bonferroni post-tests were performed considering $^{**}P < 0.01$.

(Furumai *et al.*, 2001). In accordance with this hypothesis, CG-4 cells (a glioma cancer cells) presented increased acetylation levels of their microtubule network after treatment with 1 μM TSA (Mangas-Sanjuan *et al.*, 2014). Considering the effect of HDACi on tubulin acetylation, emphasis has been given to TST, which selectively inhibits the HDAC6, a cytosolic enzyme. In human breast cancer cells, TST enhances microtubule acetylation and increases its stability, thus suppressing individual microtubule dynamics (Asthana *et al.*, 2013).

In this study, morphological changes in *T. cruzi* epimastigotes can be attributed to tubulin hyperacetylation, which may have induced microtubule cytoskeleton reorganization. Thus, several atypical phenotypes were observed, such as parasites presenting a rounding central region, as well as cell body torsion and membrane projections at the posterior end. An investigation using the negative staining technique in TSA-treated protozoa revealed that the subpellicular microtubules seemed more distanced from each other and also presented a modified orientation when compared with the control group. Because of the accumulation of acetyl radicals, it is possible that proteins that associate neighbour microtubules or that link microtubules to the membrane had their activity altered or even prevented. The causal relationship between tubulin acetylation and microtubule stability is still not clear, but it has been discussed that deacetylase inhibitors may increase HDAC6 binding to microtubules. Thus, this enzyme would act as a microtubule-associated protein, capable of affecting cytoskeleton dynamism (Asthana *et al.*, 2013).

It was interesting to observe, by fluorescence microscopy, that the posterior end of the parasites was faintly labelled with anti-acetylated tubulin. This is associated with the fact that this region contains the plus end of microtubules, usually more dynamic and, thus, less acetylated. TSA-treated cells analysed by negative staining presented microtubule disruption at the posterior end of the cell body, reinforcing the idea that this structure is less stable in this region. In *T. brucei*, the RNAi knockdown of CAP51, a protein found in association with subpellicular microtubules, also promoted microtubule rearrangement. Enlargement of the central region of the cell body was reported, a phenotype observed herein in TSA-treated parasites (Portman and Gull, 2014).

Our data obtained by flow cytometry clearly showed that microtubule acetylation increased after TSA treatment and it is associated with the fact that parasites showed cell body enlargement, as observed by negative staining images. Some studies have showed that TSA increased dramatically tubulin acetylation on cancer cells, while the induction of acetylated histone was considerably smaller (Androutsopoulos and Spandidos, 2017). Furthermore, TSA has been related to the orientation of the microtubule organizing centre (Serrador *et al.*, 2004), acetylation of protein involved in mitotic spindle assembly (Park *et al.*, 2017) and cell motility impairment (Parab *et al.*, 2015). Thus, these data give us support to suggest that TSA induces microtubule cytoskeleton remodelling in *T. cruzi*. Nevertheless, *T. cruzi* microtubules may not be the main target of TSA, since the proteomic analysis pointed to alterations on histone acetylation, showing that the nucleus is also a cellular target of this compound. Based on that, it should take into account that on this parasite the mechanism of action of TSA may not be totally dependent on tubulin.

A coordinated duplication of nuclear and kinetoplast DNA during the S phase of the cell cycle is observed in *T. cruzi* epimastigotes. After kDNA replication, the kinetoplast assumes a more elongated disk shape and segregates at the beginning of the G2 phase. At that moment, cells present two basal bodies, both linked to the kDNA network (Elias *et al.*, 2007). TSA treatment caused

https://doi.org/10.1017/S0031182018001828 Published online by Cambridge University Press

an atypical division pattern during *T. cruzi* cell cycle, namely the occurrence of multinucleated parasites containing two nuclei and one kinetoplast. Another interesting effect observed herein was the presence of parasites presenting replicated kDNA, associated with basal bodies, but without completing its segregation. It is worth mentioning that the treatment of *T. cruzi* with compounds that affect the parasite cytoskeleton, such as colchicine and taxol, is related to the occurrence of multiple organelles, atypical division patterns (two nuclei and one kinetoplast) and cytokinesis impairment (Baum *et al*., 1981; Potenza and Tellez-Iñón, 2015).

This indicates that TSA somehow promotes the stabilization between kDNA and basal bodies, which are composed by microtubules, thus impairing parasite cytokinesis. This may be related to the enhancement of microtubule acetylation, resulting in an increased number of *T. cruzi* epimastigote-treated cells in the G2/M phase.

The inhibition of HDACs by TSA has been described in cancer cell lines and human pathogens (Bauer *et al*., 2016; Altieri *et al*., 2017; Garmpis *et al*., 2017). However, acetylation of non-histone proteins represents another important target that may regulate many essential cell functions, including protein–protein interactions and protein stability.

Conclusions

In the present study, we demonstrated for the first time that TSA affects microtubules in trypanosomatids, as evidenced by cytoskeleton remodelling and cytokinesis impairment. Our results reveal new concepts regarding microtubule cytoskeleton organization and structure in trypanosomatids. In the future, further assays are necessary to prove that this compound acts as a dual inhibitor by blocking protein deacetylase activity, both in the nucleus and cytosol.

Author ORCIDs. Aline Araujo Zuma http://orcid.org/0000-0002-1286-7045.

Acknowledgements. This work was supported by Fundação Carlos Chagas Filho de Amparo à Pesquisa do Estado do Rio de Janeiro (FAPERJ) and Conselho Nacional de Desenvolvimento Científico e Tecnológico (CNPq).

References

Alonso VL and Serra EC (2012) Lysine acetylation: elucidating the components of an emerging global signaling pathway in trypanosomes. *Journal of Biomedicine and Biotechnology* **3**, 1–16.

Alonso VL, Villanova GV, Ritagliati C, Motta MCM, Cribb P and Serra EC (2014) *Trypanosoma cruzi* bromodomain factor 3 binds acetylated α-tubulin and concentrates in the flagellum during metacyclogenesis. *Eukaryotic Cell* **13**, 822–831.

Alonso VL, Ritagliati C, Cribb P, Cricco JA and Serra EC (2016) Overexpression of bromodomain factor 3 in *Trypanosoma cruzi* (TcBDF3) affects differentiation of the parasite and protects it against bromodomain inhibitors. *FEBS Journal* **283**, 2051–2066.

Alsford S and Horn D (2004) Trypanosomatid histones. *Molecular Microbiology* **53**, 365–372.

Alsford S and Horn D (2011) Elongator protein 3b negatively regulates ribosomal DNA transcription in African trypanosomes. *Molecular and Cellular Biology* **31**, 1822–1832.

Altieri F, Di Stadio CS, Federico A, Miselli G, De Palma M, Rippa E and Arcari P (2017) Epigenetic alterations of gastrokine 1 gene expression in gastric cancer. *Oncotarget* **7**, 16899–16911.

Andrews KT, Gupta AP, Tran TN, Fairlie DP, Gobert GN and Bozdech Z (2012) Comparative gene expression profiling of *P. falciparum* malaria parasites exposed to three different histone deacetylase inhibitors. *PLoS ONE* **7**, 1–9.

Androutsopoulos VP and Spandidos DA (2017) Antiproliferative effects of TSA, PXD-101 and MS-275 in A2780 and MCF7 cells: acetylated histone H4 and acetylated tubulin as markers for HDACi potency and selectivity. *Oncology Reports* **38**, 3412–3418.

Angiolilli C, Baeten DL, Radstake TR and Reedquist KA (2017) The acetyl code in rheumatoid arthritis and other rheumatic diseases. *Epigenomics* **9**, 447–461.

Asthana J, Kapoor S, Mohan R and Panda D (2013) Inhibition of HDAC6 deacetylase activity increases its binding with microtubules and suppresses microtubule dynamic instability in MCF-7 cells. *Journal of Biological Chemistry* **2**, 22516–22526.

Bauer I, Varadarajan D, Pidroni A, Gross S, Vergeiner S, Faber B, Hermann M, Tribus M, Brosch G and Graessle S (2016) A class 1 histone deacetylase with potential as an antifungal target. *Molecular Biology* **1**, 1–13.

Baum SG, Wittner M, Nadler JP, Horwitz SB, Dennis JE, Schiff PB and Tanowitz HB (1981) Taxol, a microtubule stabilizing agent, blocks the replication of *Trypanosoma cruzi*. *Proceedings of the National Academy of Sciences* **78**, 4571–4575.

Bringaud F, Reviere L and Coustou V (2006) Energy metabolism of trypanosomatids: adaptation to available carbon sources. *Molecular and Biochemical Parasitology* **149**, 1–9.

Camargo EP (1964) Growth and differentiation in *Trypanosoma cruzi*. I. Origin of metacyclic trypanosomes in liquid media. *Revista do Instituto de Medicina Tropical de São Paulo* **6**, 93–100.

Cambray-Deakin MA and Burgoyne RD (1987) Posttranslational modifications of α-tubulin: acetylated and detyrosinated forms in axons of rat cerebellum. *Journal of Cell Biology* **104**, 1569–1574.

Campo VA (2017) Comparative effects of histone deacetylases inhibitors and resveratrol on *Trypanosoma cruzi* replication, differentiation, infectivity and gene expression. *International Journal for Parasitology: Drugs and Drug Resistance* **7**, 23–33.

Cazzulo JJ (1992) Aerobic fermentation of glucose by trypanosomatids. *Federation of American Societies for Experimental Biology Journal* **6**, 3153–3161.

Chao MW, Lai MJ, Liou JP, Chang YL, Wang JC, Pan SL and Teng CM (2015) The synergic effect of vincristine and vorinostat in leukemia in vitro and in vivo. *Journal of Hematology & Oncology* **8**, 82.

Clayton C and Shapira M (2007) Post-transcriptional regulation of gene expression in trypanosomes and leishmanias. *Molecular and Biochemical Parasitology* **156**, 93–101.

Da Cunha JPC, Nakayasu ES, De Almeida IC and Schenkman S (2006) Post-translational modifications of *Trypanosoma cruzi* histone H4. *Molecular and Biochemical Parasitology* **150**, 268–277.

De Jesus TC, Nunes VS, Lopes MDEC, Martil DE, Iwai LK, Moretti NS, Machado FC, De Lima-Stein ML, Thiemann OH, Elias MC, Janzen C, Schenkman S and Da Cunha JP (2016) Chromatin proteomics reveals variable histone modifications during the life cycle of *Trypanosoma cruzi*. *Journal of Proteomics Research* **15**, 2039–2051.

De Souza W (2002) Basic cell biology of *Trypanosoma cruzi*. *Current Pharmaceutical Design* **8**, 269–285.

Ehrenkaufer GM, Eichinger DJ and Singh U (2007) Trichostatin A effects on gene expression in the protozoan parasite *Entamoeba histolytica*. *BMC Genomics* **8**, 216.

Elias MC, Da Cunha JPC, De Faria FP, Mortara RA, Freymüller E and Schenkman S (2007) Morphological events during the *Trypanosoma cruzi* cell cycle. *Protist* **158**, 147–157.

Fan J, Krautkramer KA, Feldman JL and Denu JM (2015) Metabolic regulation of histone post-translational modifications. *ACS Chemical Biology* **16**, 95–108.

Furumai R, Komatsu Y, Nishino N, Khochbin S, Yoshida M and Horinouchi S (2001) Potent histone deacetylase inhibitors built from trichostatin A and cyclic tetrapeptide antibiotics including trapoxin. *PNAS* **2**, 87–92.

García-Salcedo JA, Gijón P, Nolan DP, Tebabi P and Pays E (2003) A chromosomal SIR2 homologue with both histone NAD-dependent ADP-ribosyltransferase and deacetylase activities is involved in DNA repair in *Trypanosoma brucei*. *EMBO Journal* **22**, 5851–5862.

Garmpis N, Damaskos C, Garmpi A, Dimitroulis D, Spartalis E, Margonis GA, Schizas D, Deskou I, Doula C, Magkouti E, Andreatos N, Antoniou EA, Nonni A, Kontzoglou K and Mantas D (2017) Targeting histone deacetylases in malignant melanoma: a future therapeutic agent or just great expectations? *Anticancer Research* **37**, 5355–5362.

Henriques C, Moreira TLB, Maia-Brigagão C, Henriques-Pons A, Carvalho TMU and De Souza W (2011) Tetrazoluim salt based methods

https://doi.org/10.1017/S0031182018001828 Published online by Cambridge University Press

for high-throughput evaluation of anti-parasite chemotherapy. *Analytical Methods* **3**, 2148–2155.

Janzen CJ, Fernandez JP, Deng H, Diaz R, Hake SB and Cross GAM (2006) Unusual histone modifications in *Trypanosoma brucei*. *FEBS Letters* **580**, 2306–2310.

Jones-Brando L, Torrey EF and Yolken R (2003) Drugs used in the treatment of schizophrenia and bipolar disorder inhibit the replication of *Toxoplasma gondii*. *Schizophrenia Research* **62**, 237–344.

Khorasanizadeh S (2004) The nucleosome: from genomic organization to genomic regulation. *Cell* **116**, 259–272.

Kohl L and Gull K (1998) Molecular architecture of the trypanosome cytoskeleton. *Molecular and Biochemical Parasitology* **93**, 1–9.

L'hernault SW and Rosenbaumt JL (1985) *Chlamydomonas*α-tubulin is post-translationally modified by acetylation on the ϵ-amino group of a lysine. *Biochemistry* **24**, 473–478.

Legartová S, Stixová L, Strnad H, Kozubek S, Martinet N, Dekker FJ, Franek M and Bártová E (2013) Basic nuclear processes affected by histone acetyltransferases and histone deacetylase inhibitors. *Epigenomics* **5**, 379–396.

Mangas-Sanjuan V, Oláh J, Gonzalez-Alvarez I, Lehotzky A, Tőkési N, Bermejo M and Ovádi J (2014) Tubulin acetylation promoting potency and absorption efficacy of deacetylase inhibitors. *British Journal of Pharmacology* **172**, 829–840.

Marks PA, Richon VM, Miller T and Kelly WK (2004) Histone deacetylase inhibitors. *Advances in Cancer Research* **91**, 137–168, 2004.

Martínez-Iglesias O, Ruiz-Llorente L, Sánchez-Martínez R, García L, Zambrano A and Aranda A (2008) Histone deacetylase inhibitors: mechanism of action and therapeutic use in cancer. *Clinical and Translational Oncology* **10**, 395–398.

Monneret C (2005) Histone deacetylase inhibitors. *European Journal of Medicinal Chemistry* **40**, 1–13.

Parab S, Shetty O, Gaonkar R, Balasinor N, Khole V and Parte P (2015) HDAC6 deacetylates alpha tubulin in sperm and modulates sperm motility in Holtzman rat. *Cell and Tissue Research* **359**, 665–678.

Park I, Kwon MS, Paik S, Kim H, Lee HO, Choi E and Lee H (2017) HDAC2/3 binding and deacetylation of BubR1 initiates spindle assembly checkpoint silencing. *FEBS Journal* **284**, 035–4050.

Piperno G and Fuller MT (1985) Monoclonal antibodies specific for an acetylated form of α-tubulin recognize the antigen in cilia and flagella from a variety of organisms. *Journal of Cell Biology* **101**, 1–10.

Portman N and Gull K (2014) Identification of paralogous life-cycle stage specific cytoskeletal proteins in the parasite *Trypanosoma brucei*. *PLoS ONE* **9**, 1–9.

Potenza M and Tellez-Iñón MT (2015) Colchicine treatment reversibly blocks cytokinesis but not mitosis in *Trypanosoma cruzi* epimastigotes. *Parasitology Research* **114**, 641–649.

Robinson DR, Sherwin T, Ploubidou A, Byard EH and Gull K (1995) Microtubule polarity and dynamics in the control of organelle positioning, segregation, and cytokinesis in the trypanosome cell cycle. *Journal of Cell Biology* **128**, 1163–1172.

Sadoul K and Khochbin S (2016) The growing landscape of tubulin acetylation: lysine 40 and many more. *Biochemical Journal* **473**, 1859–1868.

Schneider A, Plessmann U and Weber K (1997) Subpellicular and flagellar microtubules of *Trypanosoma brucei* are extensively glutamylated. *Journal of Cell Science* **110**, 431–437.

Serrador JM, Cabrero JR, Sancho D, Mittelbrunn M, Urzainqui A and Sánchez-Madrid F (2004) HDAC6 deacetylase activity links the tubulin cytoskeleton with immune synapse organization. *Immunity* **20**, 417–428.

Sheader K, Te Vruchte D and Rudenko G (2004) Bloodstream form-specific up-regulation of silent VSG expression sites and procyclin in *Trypanosoma brucei* after inhibition of DNA synthesis or DNA damage. *Journal of Biological Chemistry* **2**, 13363–13374.

Soares MJ (1999) The reservosome of *Trypanosoma cruzi* epimastigotes: an organelle of the endocytic pathway with a role on metacyclogenesis. *Memórias do Instituto Oswaldo Cruz* **94**, 139–141.

Song Y and Brady ST (2015) Post-translational modifications of tubulin: pathways to functional diversity of microtubules. *Trends in Cell Biology* **25**, 125–136.

Souto-Padron T, Cunha E, Silva NL and De Souza W (1993) Acetylated alpha-tubulin in *Trypanosoma cruzi*: immunocytochemical localization. *Memórias do Instituto Oswaldo Cruz* **4**, 517–528.

Sun S, Han Y, Liu J, Fang Y, Tian Y, Zhou J, Ma D and Wu P (2014) Trichostatin A targets the mitochondrial respiratory chain, increasing mitochondrial reactive oxygen species production to trigger apoptosis in human breast cancer cells. *PLoS ONE* **9**, 1–9.

Suzuki T, Yokozaki H, Kuniyasu H, Hayashi K, Naka K, Ono S, Ishikawa T, Tahara E and Yasui W (2000) Effect of trichostatin A on cell growth and expression of cell cycle-and apoptosis-related molecules in human gastric and oral carcinoma cell lines. *International Journal of Cancer* **88**, 992–997.

Szyk A, Deaconescu AM, Spector J, Goodman B, Valenstein ML, Ziolkowska NE, Kormendi V, Grigorieff N and Roll-Mecak A (2014) Molecular basis for age-dependent microtubule acetylation by tubulin acetyltransferase. *Cell* **157**, 1405–1415.

Tavares J, Ouaissi A, Santarém N, Sereno D, Vergnes B, Sampaio P and Cordeiro-Da-Silva A (2008) The *Leishmania infantum* cytosolic SIR2-related protein 1 (LiSIR2RP1) is an NAD + -dependent deacetylase and ADP-ribosyltransferase. *Biochemical Journal* **415**, 377–386.

Thatcher TH and Gorovsky MA (1994) Phylogenetic analysis of the core histones H2A, H2B, H3, and H4. *Nucleic Acids Research* **22**, 174–179.

Toro GC and Galanti N (1990) *Trypanosoma cruzi* histones. Further characterization and comparison with higher eukaryotes. *Biochemical International* **21**, 481–490.

Toth KF (2004) Trichostatin A-induced histone acetylation causes decondensation of interphase chromatin. *Journal of Cell Science* **117**, 4277–4287.

Tsuji N, Kobayashi M, Nagashima K, Wakisaka Y and Koizumi KA (1976) New antifungal antibiotic, trichostatin. *The Journal of Antibiotics* **29**, 1–6.

Vidal JC and De Souza W (2017) Morphological and functional aspects of cytoskeleton of trypanosomatids. *Cytoskeleton – Structure, Dynamics, Function and Disease*. doi: 10.5772/66859.

Villén J and Gygi SP (2008) The SCX/IMAC enrichment approach for global phosphorylation analysis by mass spectrometry. *National Protocols* **3**, 1630–1638.

Wilson DW, Langer C, Goodman CD, Mcfadden GI and Beeson JG (2013) Defining the timing of action of antimalarial drugs against *Plasmodium falciparum*. *Antimicrobial Agents and Chemotherapy* **57**, 1455–1467.

Wloga D, Joachimiak E, Louka P and Gaertig J (2017) Posttranslational modifications of tubulin and cilia. *Cold Spring Harbor Perspectives in Biology* **9**, 1–15.

Wu Z, Zhang R, Chao C, Zhang J and Zhang Y (2007) Histone deacetylase inhibitor trichostatin A induced caspase-independent apoptosis in human gastric cancer cell. *Chinese Medical Journal* **120**, 2112–2118.

Yahiaoui B, Taibi A and Ouaissi AA (1996) *Leishmania major* protein with extensive homology to silent information regulator 2 of *Saccharomyces cerevisiae*. *Gene* **169**, 115–118.

Yang DH, Lee JW, Lee J and Moon EY (2014) Dynamic rearrangement of F-actin is required to maintain the antitumor effect of trichostatin A. *PLoS ONE* **20**, 1–8.

Zou XM, Li YL, Wang H, Cui W, Li XL, Fu SB and Jiang HC (2008) Gastric cancer cell lines induced by trichostatin A. *World Journal of Gastroenterology* **14**, 4810–4815.

Zuma AA, Mendes IC, Reignault LC, Elias MC, De Souza W, Machado CR and Motta MCM (2014) How *Trypanosoma cruzi* handles cell cycle arrest promoted by camptothecin, a topoisomerase I inhibitor. *Molecular and Biochemical Parasitology* **193**, 93–100.

https://doi.org/10.1017/S0031182018001828 Published online by Cambridge University Press